8672 *Biochemistry* **2009,** *48,* 8672–8683
DOI: 10.1021/bi901025v

BIOCHEMISTRY
including biophysical chemistry & molecular biology
Article

Crystal Structure and Acyl Chain Selectivity of *Escherichia coli* LpxD, the *N*-Acyltransferase of Lipid A Biosynthesis[†,‡]

Craig M. Bartling and Christian R. H. Raetz*

Department of Biochemistry, Duke University Medical Center, Durham, North Carolina 27710

Received June 17, 2009; Revised Manuscript Received August 4, 2009

ABSTRACT: LpxD catalyzes the third step of lipid A biosynthesis, the *R*-3-hydroxyacyl-ACP-dependent *N*-acylation of UDP-3-*O*-(acyl)-α-D-glucosamine, and is a target for new antibiotic development. Here we report the 2.6 Å crystal structure of the *Escherichia coli* LpxD homotrimer (EcLpxD). As is the case in *Chlamydia trachomatis* LpxD (CtLxpD), each EcLpxD chain consists of an *N*-terminal uridine-binding region, a left-handed parallel *β*-helix (L*β*H), and a *C*-terminal α-helical domain. The backbones of the L*β*H domains of the two enzymes are similar, as are the positions of key active site residues. The *N*-terminal nucleotide binding domains are oriented differently relative to the L*β*H regions, but are similar when overlaid on each other. The orientation of the EcLpxD tripeptide (residues 303−305), connecting the distal end of the L*β*H and the proximal end of the *C*-terminal helical domains, differs from its counterpart in CtLpxD (residues 311−312); this results in a 120° rotation of the *C*-terminal domain relative to the L*β*H region in EcLpxD versus CtLpxD. M290 of EcLpxD appears to cap the distal end of a hydrophobic cleft that binds the acyl chain of the *R*-3-hydroxyacyl-ACP donor substrate. Under standard assay conditions, wild-type EcLpxD prefers *R*,*S*-3-hydroxymyristoyl-ACP over *R*,*S*-3-hydroxypalmitoyl-ACP by a factor of 3, whereas the M290A mutant has the opposite selectivity. Both wild-type and M290A EcLpxD rescue the conditional lethality of *E. coli* RL25, a temperature-sensitive strain harboring point mutations in *lpxD*. Complementation with wild-type EcLpxD restores normal lipid A containing only *N*-linked hydroxymyristate to RL25 at 42 °C, as judged by mass spectrometry, whereas the M290A mutant generates multiple lipid A species containing one or two longer hydroxy fatty acids in place of the usual *R*-3-hydroxymyristate at positions 2 and 2′.

LpxD catalyzes the third step of lipid A biosynthesis, the acyl-ACP dependent *N*-acylation of the intermediate UDP-3-*O*-(acyl)-α-D-glucosamine (Scheme 1) (*1*−*4*). LpxD is conserved among all Gram-negative bacteria that make lipid A and is required for growth (*1*−*4*). It is therefore an excellent target for the development of new antibiotics. Three related crystal structures of LpxD from *Chlamydia trachomatis* (CtLpxD[1]) have recently been reported by Buetow et al. (*5*): an "apo" structure at 2.7 Å resolution, and two structures with bound UDP-*N*-acetylglucosamine (UDP-GlcNAc) at 2.2 Å and 3.1 Å resolution (termed Complex I and Complex II, respectively) (*5*). These structures revealed that CtLpxD contains three nearly identical protein chains within its asymmetric unit (*5*), which coincide with the three subunits of the biologically active homotrimer (Figure 1A and 1C). Furthermore, each chain of LpxD consists of three distinct regions: an *N*-terminal uridine-binding domain, a central left-handed parallel *β*-helix (L*β*H), and a *C*-terminal α-helix (Figure 2A) (*5*). All three CtLpxD structures also contain electron density suggestive of one free fatty acid bound per subunit (*5*), which was modeled as palmitate (Figures 1A and 1C); it is situated in a hydrophobic cleft located between adjacent monomers of the L*β*H domains (*5*) (Figures 1A and 1C). Complexes I and II furthermore contain one or two molecules of bound UDP-GlcNAc per homotrimer, respectively (*5*). However, neither UDP-GlcNAc nor palmitate is a physiological substrate for LpxD (*1*).

Both EcLpxD and CtLpxD catalyze the *N*-acylation of UDP-3-*O*-(acyl)-α-D-glucosamine (Scheme 1), but each orthologue appears to have a different substrate selectivity. When assayed *in vitro*, EcLpxD prefers *R*-3-hydroxymyristoyl-ACP as the acyl donor (Scheme 1A), and it utilizes UDP-3-*O*-(*R*-3-hydroxymyristoyl)-α-D-glucosamine as the acceptor (*1*, *4*). This pattern is consistent with the structure of wild-type *E. coli* lipid A, which contains over 95% *R*-3-hydroxymyristate at the 2 and 2′ positions of lipid A (Scheme 1) (*3*, *6*−*10*). CtLpxD is expected to utilize *R*-3-hydroxyarachidoyl-ACP and UDP-3-*O*-(myristoyl)-α-D-glucosamine (Scheme 1B), based on the predominant molecular species of *C. trachomatis* lipid A (*11*, *12*), but this proposal has not been validated by *in vitro* assays. Previous kinetic and site directed mutagenesis studies of EcLpxD (*4*) strongly suggested that the conserved H239 residue (corresponding to H247 in CtLpxD) (*5*) functions as the catalytic base (Scheme 2). The G257 residue of EcLpxD, which is likewise conserved in all LpxD

[†]This research was supported by NIH Grant GM-51310 to C.R.H.R. and the LIPID MAPS Large Scale Collaborative Grant GM-069338.

[‡]Atomic coordinates for EcLpxD have been deposited with the Protein Data Bank (ID code 3EH0).

*Author to whom correspondence should be addressed. Tel: (919) 684-3384. Fax: (919) 684-8885. E-mail: raetz@biochem.duke.edu.

[1]Abbreviations: ACP, acyl carrier protein; CtLpxD, *Chlamydia trachomatis* LpxD; DTT, dithiothreitol; EcLpxA, *Escherichia coli* LpxA; EcLpxD, *Escherichia coli* LpxD; Kdo, 2-keto-3-deoxy-D-*manno*-octulosonic acid; MES, 2-(*N*-morpholino)-ethanesulfonic acid; L*β*H, left-handed parallel *β* helix; LPS, lipopolysaccharide; ESI/MS, electrospray ionization mass spectrometry; PBS, phosphate-buffered saline; UDP-3-*O*-(*R*-3-hydroxymyristoyl)-GlcN, UDP-3-*O*-(*R*-3-hydroxymyristoyl)-α-D-glucosamine; UDP-3-*O*-(myristoyl)-GlcN, UDP-3-*O*-(myristoyl)-α-D-glucosamine; UDP-GlcNAc, UDP-*N*-acetylglucosamine.

 Published on Web 08/05/2009

Scheme 1: Selectivity and Function of EcLpxD versus CtLpxD

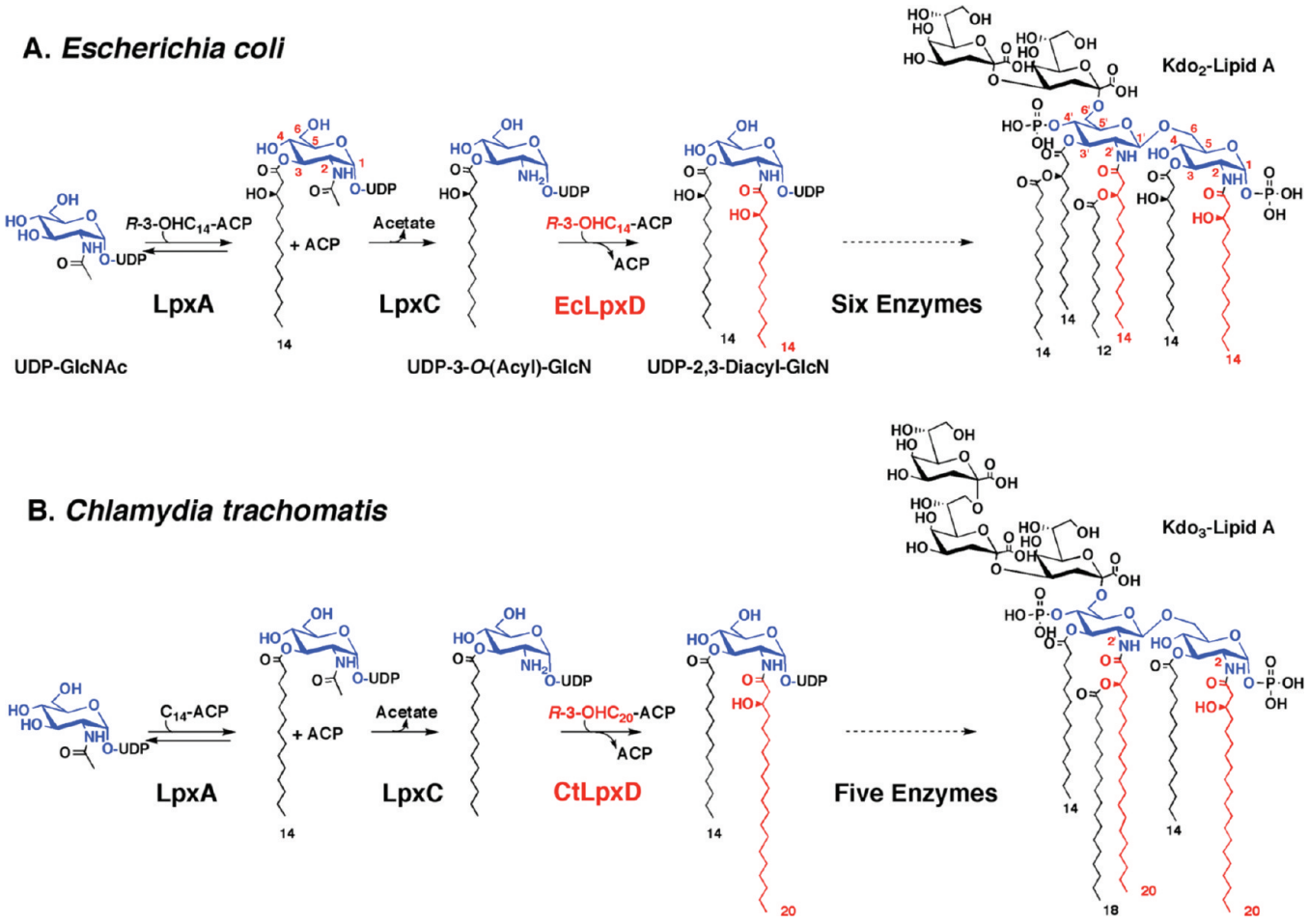

orthologues, is located near H239, and its backbone amide group may function as the oxyanion hole (Scheme 2) (*4*). Kinetic and mutagenesis studies of CtLpxD have not been reported.

Here we present the first crystal structure of EcLpxD, which was determined by molecular replacement using CtLpxD (pdb code 2IUA) as the model (*5*) in conjunction with primary sequence alignments. Overall, the structure of EcLpxD is similar to that of CtLpxD, but significant differences exist in the connections between the three domains of each chain. Comparison of the two enzymes also revealed differences in the size of a hydrophobic cleft that extends from the catalytic histidine residue and may function in determining the *R*-3-hydroxyacyl-ACP selectivity of LpxD. We therefore constructed the M290A mutation, which is predicted to enlarge this hydrophobic cleft in EcLpxD. Introduction of the M290A variant into a recipient strain of *E. coli* harboring a temperature-sensitive *lpxD* point mutation (*13*) greatly enhances the incorporation of longer hydroxyacyl chains into lipid A in living cells and is accompanied by corresponding changes in the acyl donor selectivity of LpxD, when assayed *in vitro*.

EXPERIMENTAL PROCEDURES

Materials. [α-^{32}P]-UTP was purchased from Perkin-Elmer (Boston, MA). The crystallography reagents 2-(*N*-morpholino)ethanesulfonic acid (MES), ammonium sulfate, dioxane, sodium chloride, and ethylene glycol were purchased from Hampton Research (Aliso Viejo, CA). Ni-NTA resin was purchased from GE Healthcare (Piscataway, NJ). All other chemicals were purchased from Sigma-Aldrich (St. Louis, MO) or prepared as described below.

EcLpxD Expression and Purification. A plasmid (designated pNH6LpxD), which encodes a fully functional LpxD protein, modified with an *N*-terminal His_6 tag followed by a one glycine residue linker and the P2A substitution, was constructed and transformed into *E. coli* Rosetta (DE3)/pLysS (Invitrogen), as previously described (*4*). Expression of LpxD at 37 °C was induced for 3.5 h with 1 mM isopropyl-β-D-thiogalactopyranoside when the A_{600} of the cells, growing on LB broth supplemented with 25 μg/mL chloramphenicol and 100 μg/mL ampicillin, reached 0.5. All subsequent procedures were carried out at 0−4 °C. Cells from a 1 L culture were harvested by centrifugation at 4000*g*. The pellet was resuspended in 50 mL of buffer A (40 mM potassium phosphate, pH 8.0, containing 200 mM sodium chloride, 1 mM DTT, 10% glycerol [v/v] supplemented with 20 mM imidazole), and the cells were again centrifuged at 4000*g*. The pellet was resuspended in 50 mL of buffer A, and the cells were broken by one passage through a French pressure chamber at 18,000 psi. After a 30 min centrifugation at 4000*g*, the cell-free extract was loaded onto a 4 mL Ni-NTA column, equilibrated with 60 mL of buffer A. After washing with 40 mL of buffer A, LpxD was eluted in one fraction with 10 mL of buffer A containing 150 mM imidazole, and the entire fraction was loaded onto a 318 mL High Load 26/60 Superdex-200 gel filtration column (GE Healthcare, Piscataway, NJ), equilibrated in 10 mM Tris chloride, pH 8.0, containing 1 mM DTT and 500 mM NaCl. The protein eluted as a sharp peak

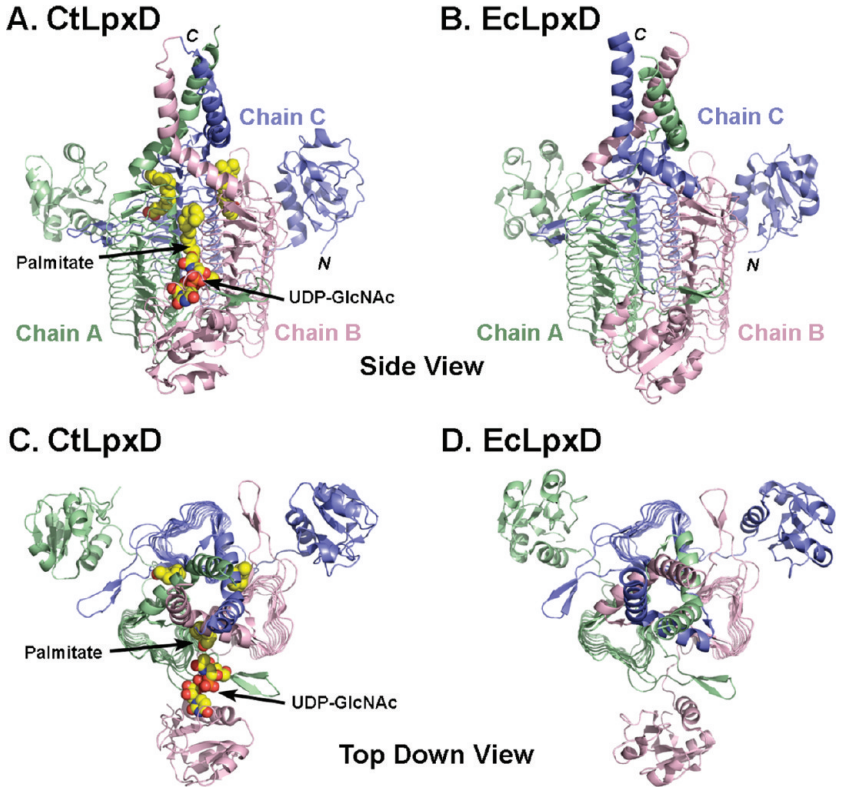

FIGURE 1: Comparison of the trimeric architecture CtLpxD (Complex I) and EcLpxD. Panels A and B show side views of the asymmetric units of CtLpxD (Complex I) (*5*) and EcLpxD, respectively. In both structures, chains A, B and C (green, pink and blue, respectively) of the asymmetric unit coincide with the three subunits of the physiologically relevant LpxD homotrimer. CtLpxD contains one molecule of bound free fatty acid per protein monomer (*5*), which is modeled as palmitate, but there is only one molecule of UDP-GlcNAc per homotrimer (carbons in yellow). The locations of the *N*- and *C*-termini are indicated for chain C. The + 120° rotation of the *C*-terminal α-helical domain relative to the LβH domain in EcLpxD versus CtLpxD is apparent in this perspective. Panels C and D show top-down views of the asymmetric units of CtLpxD (Complex I) and EcLpxD, respectively, illustrating the precise stacking of the coils of the LβH region and the dispositions of the *N*-terminal nucleotide binding domains.

consistent with the molecular weight predicted for the LpxD homotrimer. Fractions were pooled and concentrated to 24 mg/mL, as judged by the bicinchoninic acid assay (*14*). The protein solution was then passed through a 0.2 μm filter and stored in aliquots at −80 °C.

LpxD Substrate Preparation and LpxD Assay. *R*,*S*-3-Hydroxymyristoyl-ACP, *R*,*S*-3-hydroxypalmitoyl-ACP and [α-^{32}P]-UDP-3-*O*-(*R*-3-hydroxymyristoyl)-α-D-glucosamine were prepared as previously described (*1*, *4*). All assay mixtures (typically 10 μL) contained 1 μM UDP-3-*O*-(*R*-3-hydroxymyristoyl)-α-D-glucosamine, [α-^{32}P]-UDP-3-*O*-(*R*-3-hydroxymyristoyl)-α-D-glucosamine (5000 − 10000 cpm/μL), and 2 μM *R*,*S*-3-hydroxypalmitoyl-ACP or *R*,*S*-3-hydroxymyristoyl-ACP (*4*). LpxD point mutants (M290A and M292A) were constructed using pNH6LpxD as the template, and the mutant proteins were expressed and purified as previously described (*4*).

Crystallization and Structure Determination. Crystals were grown by the hanging drop/vapor diffusion method by mixing 1.7 μL of 10 mg/mL protein (in 10 mM Tris chloride, pH 8.0 containing 1 mM DTT and 500 mM NaCl) with 1.7 μL of 100 mM MES, pH 5.4, containing 2.0 M $(NH_4)_2SO_4$, 1% dioxane *v*/*v*, and 1 mM DTT. Crystals appeared after 3−5 days at 17 °C and grew to ~100 μm after two weeks in the shape of tetragonal bipyramids. Crystals were harvested with a CryoLoop (Hampton Research, Aliso Viejo, CA), and soaked for about 5 s in 100 mM MES, pH 5.4, containing 2.0 M $(NH_4)_2SO_4$, 1% dioxane v/v, 500 mM NaCl, and 18% ethylene glycol v/v, followed by submersion in liquid N_2. Data were collected using an R-Axis IV image plate detector (Rigaku, The Woodlands, TX). The EcLpxD asymmetric unit consists of three nearly identical chains, arranged in the same manner as in the biologically relevant homotrimer, with a solvent content of ~56%. Data were integrated and scaled using XDS (*15*).

The EcLpxD structure was determined by molecular replacement to 2.6 Å resolution using Phaser, a component of the CCP4 suite[2] (*16*, *17*). An initial homology model of the EcLpxD trimer was constructed based on the crystal structure of CtLpxD with all ligands and waters removed (PDB code: 2IUA), using the program Molrep (*18*). Initial solutions did not permit proper refinement; therefore, the homology model was altered by first removing the predicted loop regions of the *N*-terminal domain of CtLpxD (Table S1 in the Supporting Information). This model gave adequate phase estimates for subsequent model building, which was performed in Coot (*19*) and refined using Refmac (*20*) and Phenix (*21*). Solvent molecules were added using Phenix (*21*). The final structure of EcLpxD was assessed using MolProbity (*22*, *23*). The initial round of refinement before any rebuilding yielded initial values of R_{work} of 34.6% and R_{free} of 43.9%. Iterative rounds of refinement monitored by R_{free} yielded a model with a final R_{work} of 21.4% and R_{free} of 27.9% (Table 1). The His_6 tag and glycine linker at the *N*-terminus were not included in the model because these residues did not show sufficient electron density for model building. The final EcLpxD model has 98.6%

[2]The CCP4 suite of programs for protein crystallography is described in (1994) *Acta Crystallogr. 50*, 760−763.

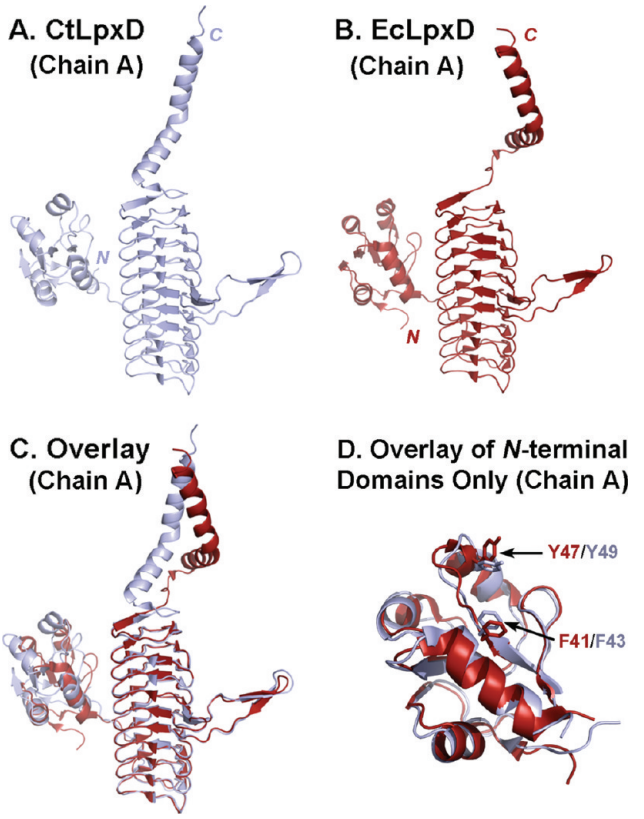

FIGURE 2: Comparison of the CtLpxD and EcLpxD monomers. Panels A and B show ribbon diagrams of chain A of CtLpxA (gray) and EcLpxD (red), respectively. The differences in the orientations of the linkers connecting the LβH and *C*-terminal domains of the two proteins are especially clear in this view. Panel C shows the superpositioned ribbon diagrams of the two proteins, demonstrating the close similarity of the central LβH domain, but the differences in the *N*-terminal and *C*-terminal regions. Panel D: When the *N*-terminal domains by themselves are superpositioned, their conformational similarities are more apparent. Aromatic side chains thought to be involved in uridine binding are indicated (*4*, *5*).

Scheme 2: Proposed Catalytic Mechanism of EcLpxD

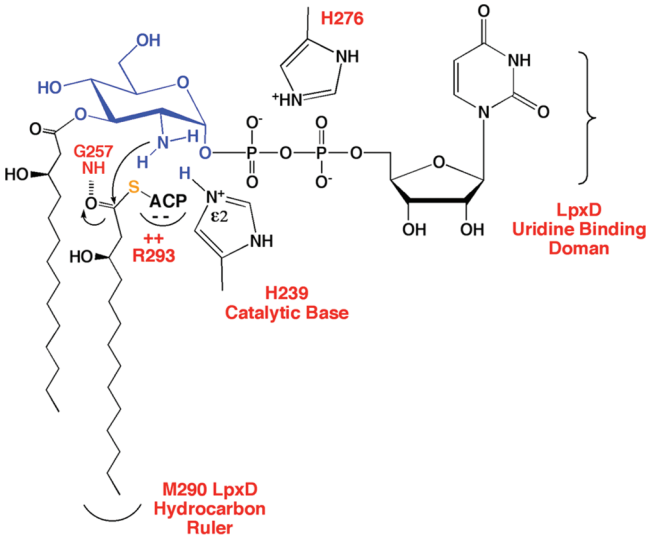

of its residues in the Ramachandran favored regions and less than 1% of the rotamers in the disallowed regions. Secondary structure elements were added with the help of the program STRIDE (*24*) and by visual inspection. Structural alignments and figures were generated using PyMol (DeLano Scientific, San Carlos, CA). Atomic coordinates for EcLpxD have been deposited with the Protein Data Bank (ID code 3EH0).

Cloning of Wild-Type and M290A lpxD for Transformation into RL25. The *E. coli lpxD* gene was previously cloned into a pET-11d plasmid (*4*). A *Hin*dIII restriction site was engineered downstream from the gene using the QuikChange site-directed mutagenesis techniques (Stratagene), and the resulting *Hin*dIII/*Xba*I doubly digested insert was subcloned into a similarly digested pBAD33 vector (*25*). The resulting plasmid, designated pWT, was used as the template to create the M290A *lpxD* variant (pM290A), using the QuikChange site-directed mutagenesis kit. The structures of all plasmid inserts were confirmed by DNA sequencing. The pBAD33, pWT, and pM290A were electroporated into RL25, a temperature-sensitive *lpxD* point mutant strain (*13*), obtained from the *E. coli* Genetic Stock Center, Yale University, New Haven, CT. Colonies were selected on LB plates (*26*) at 30 °C supplemented with 25 μg/mL chloramphenicol. RL25 cells containing pWT or pM290A, but not pBAD33, restored growth of RL25 at 42 °C, both on plates and in liquid medium. For the lipid A analysis, 200 mL LB cultures (supplemented with 25 μg/mL chloramphenicol and 0.1% L-arabinose *w*/*v*) of RL25, containing either pWT or pM290A, were grown at 30 °C to an A_{600} of 0.2, followed by a temperature shift to 42 °C. Cells were harvested when A_{600} reached 1.0.

Isolation and Characterization of Lipid A Species. Cells were harvested by centrifugation at 4000*g* and washed with 30 mL of phosphate-buffered saline, pH 7.4 (PBS). The cell pellets were resuspended in 8 mL of PBS, 10 mL of chloroform, and 20 mL of methanol to make a single-phase Bligh/Dyer system (*27*). After mixing and incubating at room temperature for 1 h, the pellet was recovered by centrifugation and washed twice with 15 mL of a single-phase Bligh/Dyer mixture (*27*). The pellet was resuspended in 9 mL of 50 mM sodium acetate, pH 4.5, and incubated at 100 °C for 30 min to cleave the Kdo−lipid A linkage (*28*). The hydrolysis mixture was cooled and acidified to pH 1.0 with concentrated HCl. The lipid A was recovered in the lower phase of a two-phase Bligh/Dyer mixture (*28*), generated by the addition of appropriate amounts of chloroform and methanol.

To remove the ester-linked fatty acids, a portion of each lipid A preparation was subjected to mild alkaline hydrolysis (*29*). About 20% of each sample was dissolved in 0.5 mL of a basic, single-phase solution, which was prepared by mixing 0.4 mL of 5 M NaOH, 5 mL of methanol and 5 mL of chloroform to yield a final concentration of ~0.2 M NaOH. This mixture was incubated at room temperature for 30 min. The base-deacylated lipid A species were then recovered from the lower phase of a two-phase, acidic Bligh/Dyer system (*28*), generated by adding appropriate amounts of chloroform and methanol.

High-resolution mass spectra were acquired in the negative ion mode on a QSTAR XL quadrupole time-of-flight tandem mass spectrometer (Applied Biosystems, Foster City, CA), equipped with an electrospray ionization source (*30*, *31*). For MS/MS analysis, tandem mass spectra were obtained using a collision energy of −35 V, with nitrogen as the collision gas. Data analysis was performed using Analyst QS software.

RESULTS

Crystal Structure of EcLpxD. The crystal structure of *N*-terminally His_6-tagged EcLpxD was determined by molecular

Table 1: Data Collection and Refinement Statistics

measurement	value
source/detector	RU200/Raxis-IV
space group	*C*2
a, *b*, *c* (Å)	157.95, 94.17, 103.66
α, *β*, *γ* (deg)	90.00, 126.50, 90.00
wavelength (Å)	1.5418
oscillation range/Δ, deg	160/ 0.5
resolution range (Å)	20.0−2.60
last shell (Å)	2.74−2.60
unique reflections	37,053
completeness (last shell)	98.3% (97.2%)
average $I/\sigma_{(I)}$ (last shell)	10.3 (3.1)
redundancy (last shell)	3.3 (3.3)
R_{merge}[a]	10.2% (44.0%)
R_{work}[b]	21.4%
R_{free}	27.9%
rms from ideality	
bond lengths, Å	0.015
bond angles, deg	1.481
protein residues	1,023
waters	365

[a] $R_{\text{merge}} = \sum_{hkl}\sum_i |I_i(hkl) - |\langle I(hkl)\rangle|/\sum_{hkl}\sum_i I(hkl)$. [b] $R_{\text{work}} = \sum|F_o - F_c|/\sum F_o$. 5% of the reflections were used to calculate R_{free}.

replacement at 2.6 Å resolution, using CtLpxD (PDB code: 2IUA) as the model (Table 1). Each chain of the EcLpxD homotrimer (excluding the *N*-terminal His_6 tag and glycine linker) consists of 341 amino acid residues, compared to 354 residues in CtLpxD. The EcLpxD and CtLpxD monomers show 33% identity and 53% similarity with 7 gaps over 330 amino acid residues (see Figure S1 in the Supporting Information). In the crystalline state, both enzymes contain three polypeptide chains per asymmetric unit, which are arranged in the same manner as in the biologically functional homotrimer (Figure 1). The conformations of each of the three monomers are very similar, and these subunits are related to each other by a 3-fold axis of symmetry (Figure 1). The His_6 tag and glycine linker of EcLpxD were not visible in the electron density maps and were not included in the model (Figure 1).

Comparison of EcLpxD and CtLpxD. Each chain of the CtLpxD (*5*) and the EcLpxD homotrimers (Figures 2A and 2B) consists of three regions: a mixed α/*β* *N*-terminal domain, a central, left-handed parallel *β*-helix (L*β*H), and an extended α-helical *C*-terminal domain. Superposition of chain A of CtLpxD[3] and chain A of EcLpxD (Figure 2C) shows the close conformational similarity of the central L*β*H regions. However, the *N*-terminal domains of CtLpxD and EcLpxD are not well aligned (Figure 2C) because of the different orientations of these domains relative to their corresponding L*β*H regions. When superpositioning only the *N*-terminal regions of CtLpxD and EcLpxD (Figure 2D), the similarity of their secondary structures and the orientations of their uridine binding aromatic side chains are more apparent (see also Table S1 in the Supporting Information). The difference in the *N*-terminal domain orientation likely arises from the fact that the segment connecting it to the L*β*H region is one amino acid shorter in EcLpxD than CtLpxD (Figure S1 and Table S1 in the Supporting Information) and might also indicate mobility of the two domains relative to each other (Figure 2C).

[3]For this purpose we used CtLpxD complex I, which was solved at 2.2 Å resolution, and contains one molecule of bound UDP-GlcNAc between chains A and B, and three molecules of bound palmitate (one at each active site).

The most striking overall difference between the two proteins is the connection between the L*β*H and the *C*-terminal regions (Figures 3A and 3B). The residues connecting the L*β*H to the *C*-terminal domains of CtLpxD (G311 and A312) and EcLpxD (S303, G304, and I305) differ in length and orientation (Figures 3A and 3B), resulting in a +120° twist of the *C*-terminal domain relative to L*β*H region in EcLpxD versus CtLpxD (Figures 1, 2 and 3). Although the role of the *C*-terminal domain is unclear, it is important for the function of the protein, because the EcLpxD *C*-terminal truncations Δ324−341 and Δ312−341 are inactive (data not shown). Constructs lacking the *C*-terminal domain can be overexpressed, as judged by gel electrophoresis, but we have not yet determined whether they fold properly and assemble into trimers.

Active Site Residues of EcLpxD. CtLpxD was crystallized in three forms, each of which contained three bound palmitate molecules situated between adjacent monomers, as shown in Figure 1 for Complex I, the highest resolution structure obtained (*5*) (PDB code: 2IU8). Complex I was crystallized with UDP-GlcNAc and contained electron density consistent with the presence of one molecule of UDP-GlcNAc between chains A and B (Figures 1A and 1C) (*5*). Palmitate was not added during the CtLpxD crystallization and must have been derived from the *E. coli* cells in which the recombinant CtLpxD was expressed (*5*). No free fatty acids were associated with EcLpxD.

Neither palmitate nor UDP-GlcNAc is a physiological substrate for LpxD (Scheme 1), but their locations within the CtLpxD structure (*5*) provide significant information about the LpxD active site. When the EcLpxD and CtLpxD (Complex I) homotrimers are superpositioned (Figure 4A), there is excellent alignment of their L*β*H backbones (CtLpxD monomers in gray and EcLpxD monomers in green, pink and blue). The conserved catalytic His residues (EcLpxD H239 and CtLpxD H247) are positioned almost identically and are poised to function as the catalytic base (Scheme 2). The conserved glycine residues that are located one turn distally toward the *C*-terminal end of the *β*-helix are proposed to function as the oxyanion hole (Scheme 2), and they also superposition very precisely (Figure 4A). The electron density in the active site region around H239 is very well-defined (Figure 4C). As shown previously (*4*), H125, the catalytic base of *E. coli* LpxA (*32*−*34*), likewise aligns well with CtLpxD H247, highlighting the related structures and mechanisms of these acyltransferases.

The Hydrophobic Cleft for the Binding an Acyl Chain. In the superpositioned active site regions of CtLpxD and EcLpxD (Figure 4A), the bound palmitate molecule present in CtLpxD is highlighted with its carbon atoms in yellow sticks. Careful comparison of these structures reveals that the M290 side chain of EcLpxD overlaps with the region occupied by the tail of the palmitate molecule present in CtLpxD (Figure 4A, 1.6 Å separation). It is unclear whether the palmitate ligand in CtLpxD is situated in the acyl chain-binding cleft of the donor or the acceptor substrate (Scheme 1). Buetow et al. (*5*) suggested that the palmitate molecule occupies the myristoyl chain binding site of the UDP-3-*O*-(C_{14})-GlcN acceptor (Scheme 1). However, the CtLpxD palmitate-binding site may be large enough to accommodate the *R*-3-hydroxyarachidoyl-ACP donor substrate (Scheme 1B). The comparable region in EcLpxD (Figure 4A) is too small to accommodate palmitate or longer acyl chains because of the positioning of the M290 side chain (Figures 4A and 4B), and possibly also because of the presence of M292 (not shown). Nevertheless, this region of EcLpxD should be large

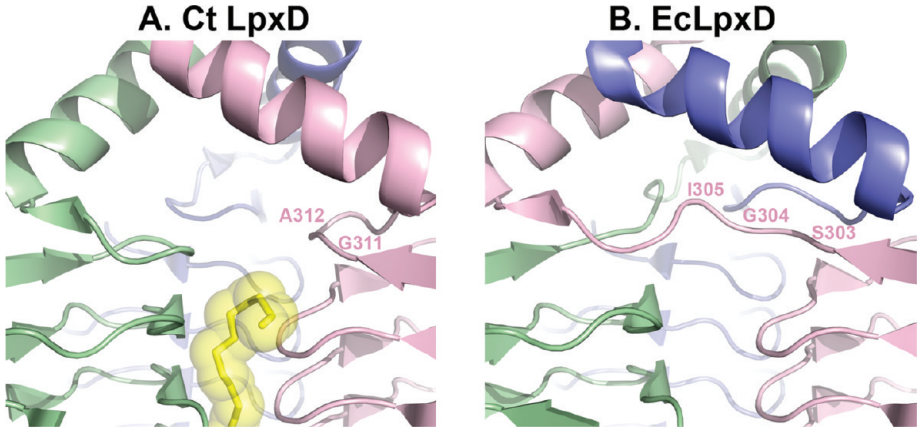

FIGURE 3: Orientation of the peptide segments connecting the LβH to the *C*-terminal domains in CtLpxD versus EcLpxD. Panels A and B magnify and highlight the orientation of relevant chain B dipeptide for CtLpxD and the corresponding tripeptide in EcLpxD, connecting the LβH to the *C*-terminal region. The color scheme is the same as in Figure 1. The end of the bound palmitate molecule present between chains A and B of CtLpxD is shown with its carbon atoms in yellow. No bound fatty acid is present in EcLpxD.

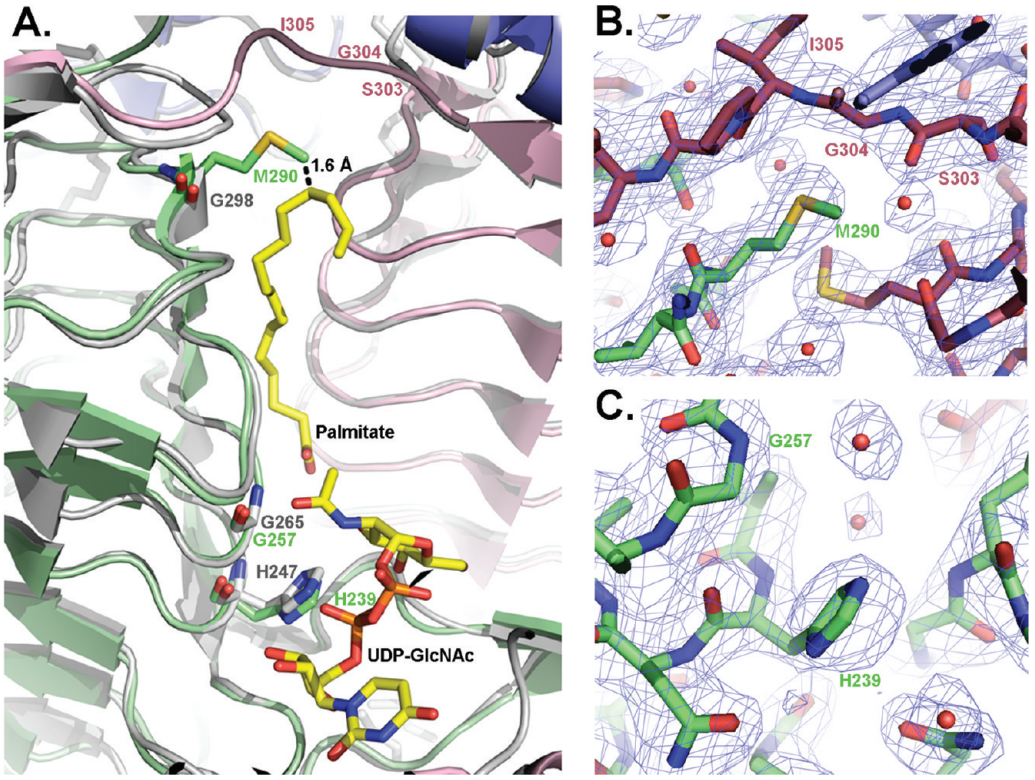

FIGURE 4: Proposed active sites and acyl chain binding clefts of CtLpxD versus EcLpxD. Panel A shows the superpositioned ribbons diagrams of CtLpxD (Complex I with its three protein monomers in gray) (*5*) and EcLpxD (chain A in green, chain B in pink, and chain C in blue). The position of the palmitate molecule between chains A and B in CtLpxA is shown in sticks, as are the catalytic base of chain A (H239 in EcLpxD and H247 in CtLpxD), the oxyanion hole (G257 in EcLpxD and G265 in CtLpxD), and the "hydrocarbon ruler" M290 of EcLpxD versus G298 of CtLpxD. The two distal carbon atoms of the palmitate chain would clash with the M290 side chain, perhaps accounting for the acyl chain selectivity of EcLpxD. Panel B shows the $2F_o - F_c$ map around the M290 residue in chain A of EcLpxD and the nearby peptide that connects the LβH and *C*-terminal regions of chain B, contoured at 1σ (see also Figure 3B). The densities of the M290 side chain and the connecting peptide are well-defined. Panel C shows the $2F_o - F_c$ map around the catalytic base H239 of chain A of EcLpxD, contoured at 1σ.

enough to accommodate the *R*-3-hydroxymyristoyl moiety of *R*-3-hydroxymyristoyl-ACP (Figure 4A). The electron densities of the M290 side chain and of the nearby peptide segment connecting the LβH region to the *C*-terminal domain of EcLpxD are well-defined (Figure 4B).

Site-Directed Mutagenesis of the Proposed Fatty Acid Binding Cleft in EcLpxD. Attempts to crystallize EcLpxD with UDP-GlcNAc, UDP-3-*O*-(*R*-3-hydroxymyristoyl)-α-D-GlcNAc or its product UDP-2,3-diacylglucosamine (Scheme 1) were unsuccessful. To show that the EcLpxD cleft corresponding to the palmitate binding region of CtLpxD (Figure 4A) interacts with the *R*-3-hydroxyacyl chain of *R*-hydroxyacyl-ACP, we constructed two EcLpxD mutants, M290A and M292A, and compared their acyl-ACP chain length selectivity *in vitro* to that of wild-type EcLpxD. The assays were performed with substrate concentrations below K_M. The selectivity factor (Table 2) approximates the k_{cat}/K_M ratios. Wild-type EcLpxD displays a 3.3-fold selectivity for *R*,*S*-3-hydroxymyristoyl-ACP

over *R*,*S*-3-hydroxypalmitoyl-ACP. A similar result was obtained for the M292A variant (Table 2). However, the M290A mutant displayed a 2.5-fold selectivity for *R*,*S*-3-hydroxypalmitoyl-ACP over *R*,*S*-3-hydroxymyristoyl-ACP (Table 2). This finding supports the view that the M290 side chain may indeed limit the size of the acyl chain binding groove of EcLpxD, as suggested by Figure 4A, favoring the selection of *R*-3-hydroxymyristoyl-ACP over longer *R*-3-hydroxyacyl-ACPs.

Effects of the M290A Mutation on Lipid A Composition in Living Cells. LpxD of *E. coli* strain RL25 (*13*, *35*) contains three point mutations, which are not located near the active site (not shown); they are compatible with cell growth at 30 °C but not 42 °C (Figure 5A) (*13*). Transformation of RL25 with plasmids expressing either wild-type EcLpxD (pWT) or the M290A variant (pM290A) restored growth of single colonies of RL25 at 42 °C (Figures 5B and 5C, respectively).

To determine which hydroxyacyl chains were incorporated into lipid A *in vivo*, RL25 cells harboring either pWT or pM290A were grown to late log phase at 42 °C. Following mild acid hydrolysis of cell-associated LPS, their lipid A species were isolated and subjected to ESI/MS in the negative ion mode (Figure 6). The $[M - 2H]^{2-}$ ion at *m*/*z* 897.62 of the major lipid A species present in RL25/pWT (Figure 6A, blue line) was the same as that of wild-type *E. coli* (not shown). The proposed structure that gives rise to this ion contains *N*-linked *R*-3-hydroxymyristoyl chains at the 2 and 2′ positions (Figure 6A, red atoms) (*30*). The smaller peak at *m*/*z* 883.60 (Figure 6A) is attributed to the $[M - 2H]^{2-}$ ion of a minor species in which the secondary myristate chain at position 3′ is replaced with a laurate moiety (*30*). The smaller peak at *m*/*z* 937.60 (Figure 6A, red line) is attributed to $[M - 2H]^{2-}$ of a lipid A species bearing a diphosphate unit at the 1-position (structure not shown) (*28*, *36*).

Table 2: Hydroxyacyl-ACP Selectivity of Purified EcLpxD Variants[a]

EcLpxD protein	sp act. (nmol/min/mg) *R*,*S*-3-OHC_{14}-ACP	sp act. (nmol/min/mg) *R*,*S*-3-OHC_{16}-ACP	selectivity ratio
wild-type	997 ± 10	300 ± 13	C_{14}/C_{16} (3.3)
M292A	84 ± 6	18 ± 3	C_{14}/C_{16} (4.7)
M290A	52 ± 5	132 ± 2	C_{16}/C_{14} (2.5)

[a]Abbreviations: *R*,*S*-3-OHC_{14}-ACP, *R*,*S*-3-hydroxymyristoyl-ACP; *R*,*S*-3-OHC_{16}-ACP, *R*,*S*-3-hydroxypalmitoyl-ACP.

The negative ion spectrum of the lipid A isolated from RL25/pM290A is more complex (Figure 6B). The peak at *m*/*z* 897.62, arising from the residual wild-type lipid A, is relatively small. Additional putative lipid A species are observed at *m*/*z* 911.64, 924.64, 925.65, 938.65 and 951.65, consistent with the $[M - 2H]^{2-}$ ions of lipid A molecules containing one or two longer hydroxyacyl chains with sixteen or eighteen carbon atoms (Figure 6B, blue lines). The peak spacing suggests that some of these longer acyl chains are unsaturated (see below). A corresponding series of larger peak is seen for the lipid A diphosphate variant (Figure 6B, red lines).

Analysis of the N-Linked Hydroxyacyl Chains of Lipid A in RL25/pM290A. To demonstrate that the longer acyl chains present in the lipid A of RL25/pM290A (Figure 6B) were incorporated by the mutant LpxD acyltransferase, the purified lipid A was subjected to mild-alkaline hydrolysis (*29*). This procedure removes all the ester-linked acyl chains (Figure 6A), but not the amide-linked *R*-3-hydroxyacyl chains at the 2 and 2′ positions, which are incorporated by LpxD (Figure 7A, inserted structures). In this experiment, both $[M - 2H]^{2-}$ ions at *m*/*z* 475.24 (black line) and $[M - H]^{-}$ ions at *m*/*z* 951.49 (blue line) were observed for the *O*-deacylated lipid A of RL25/pWT (Figure 7A, far left and right structures). The additional singly charged peak at *m*/*z* 871.52 (Figure 7A, green line) arises from lipid A molecules that lost their anomeric phosphate group during the mild acid hydrolysis used to cleave the Kdo−lipid A linkage of LPS (Figure 7A, middle structure) (*28*). These 1-dephosphorylated lipid A species are chemical artifacts, not normally present in wild-type cells.

As shown in Figure 7B, all the $[M - H]^{-}$ and $[M - 2H]^{2-}$ ions derived from the base-deacylated lipid A of RL25/pM290A display heterogeneity indicative of the presence of longer *N*-linked hydroxyacyl chains. This pattern accounts for the results obtained with the intact lipid A prior to base treatment (Figure 6B). The $[M - H]^{-}$ ions for the base deacylated lipid A species at *m*/*z* 979.56, 1005.54, 1007.55, 1033.58, and 1059.58

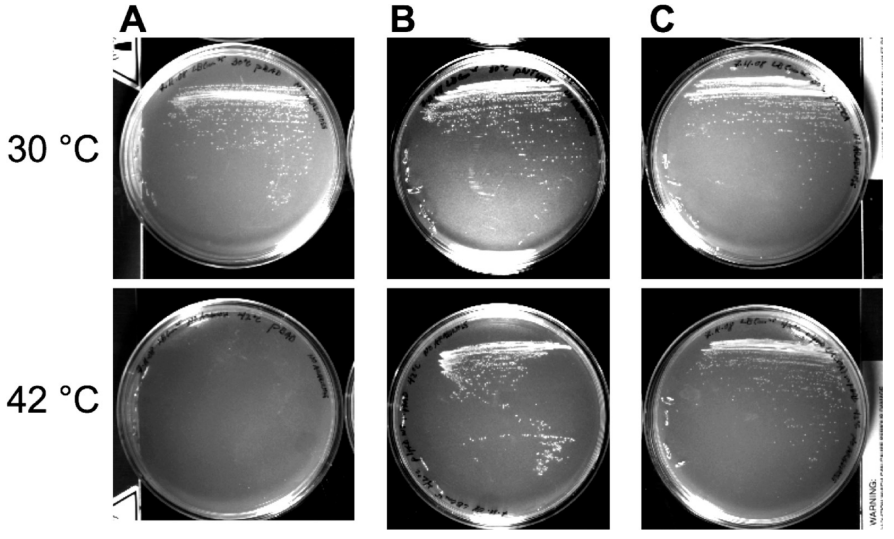

FIGURE 5: Complementation of the temperature-sensitive LpxD mutant RL25 with pWT or pM290A. Cells were streaked onto LB agar plates containing 25 μg/mL chloramphenicol and 0.1% L-arabinose and incubated overnight at 30 or 42 °C, as indicated. Panel A, RL25 harboring the vector control pBAD33. Panel B, RL25/pWT. Panel C, RL25/pM290A.

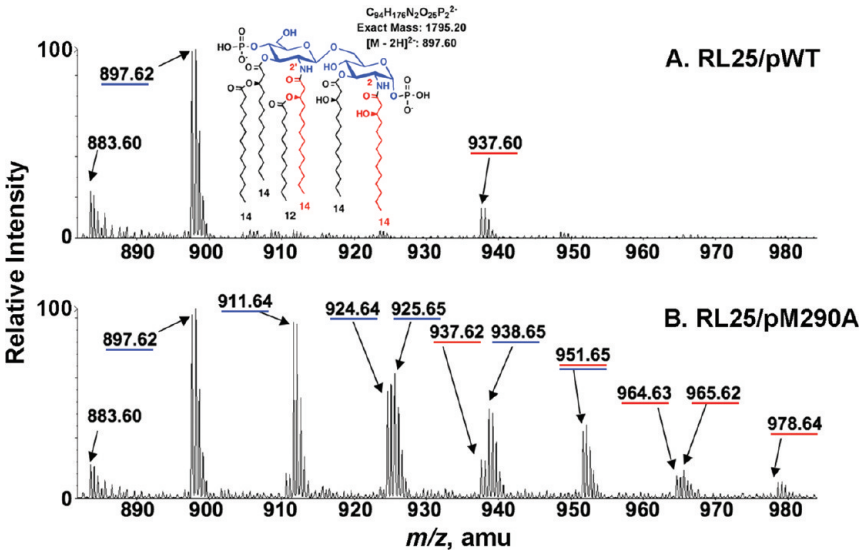

FIGURE 6: ESI/MS of lipid A from RL25 rescued at 42 °C by either pWT or pM290A. Panel A: ESI mass spectrum showing the doubly charged $[M - 2H]^{2-}$ ions of the lipid A molecules from RL25/pWT grown at 42 °C. The inset shows the structure of the predominant wild-type lipid A species giving rise to the ions at *m*/*z* 897.62. Panel B: Spectrum of the doubly charged $[M - 2H]^{2-}$ ions of the lipid A molecules from RL25/pM290A grown at 42 °C, showing a more complex pattern indicative of the incorporation of longer acyl chains. The peaks labeled with arrows correspond to predicted lipid A species containing either a monophosphate residue at the 1 position (blue lines) or a diphosphate group at the 1 position (red lines).

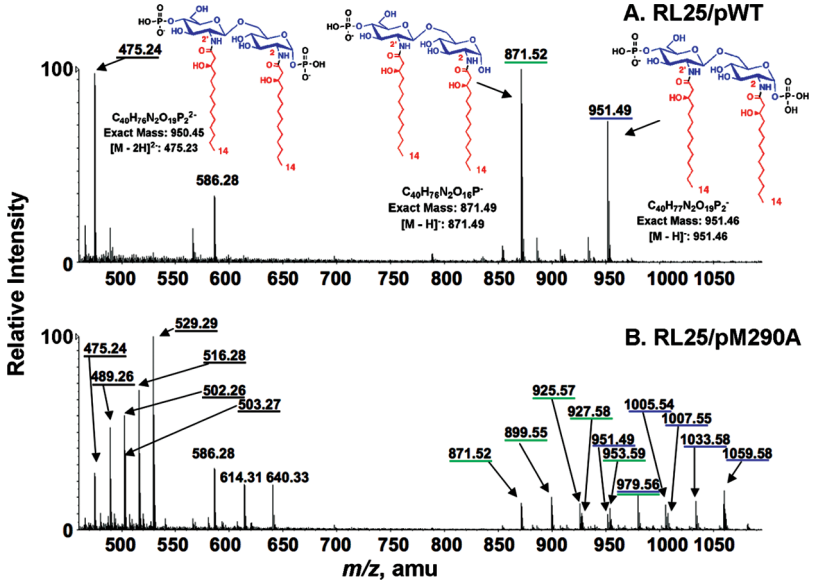

FIGURE 7: ESI/MS analysis of *O*-deacylated lipid A from RL25 rescued by pWT or pM290A. Panel A: Negative ion ESI mass spectrum of lipid A molecules from RL25/pWT grown at 42 °C. The far-right and far-left insets show the structures of the predominant wild-type *O*-deacylated lipid A species, giving rise to the singly charged ions at *m*/*z* 951.49 (blue line) and to the doubly charged ions at *m*/*z* 475.24 (black line), respectively. The peak at *m*/*z* 871.52 (green line) arises from lipid A molecules that lost their anomeric phosphate group during the mild acid hydrolysis procedure used to prepare the sample (*28*). Panel B: Corresponding spectrum of the *O*-deacylated lipid A molecules from RL25/pM290A, showing that the series of longer acyl-chains present in this material are mostly *N*-linked. Their masses are consistent with the incorporation of one or two *R*-3-hydroxypalmitate and/or *R*-3-hydroxy-*cis*-vaccenate moieties in place of *R*-3-hydroxymyristate at positions 2 and 2′. This series of longer chains are seen with both the singly (blue lines) and the doubly charged (black lines) lipid A ions, and with the 1-dephosphorylated lipid A species (green lines). The peaks noted with arrows correspond to predicted lipid A species. The remaining peaks have not been identified.

(Figure 7B, blue lines) are consistent with the incorporation of one or two longer *N*-linked hydroxyacyl chains with sixteen or eighteen carbon atoms by the LpxD variant M290A. The species at *m*/*z* 951.49 (Figure 7B, blue line) is the same as the predominant form observed in the wild-type, which contains two *R*-3-hydroxymyristate substituents (Figure 7A). The species at *m*/*z* 1007.55 (+ 56.06 amu relative to 951.49) are consistent with a lipid A molecule containing two *N*-linked *R*-3-hydroxy-palmitate units, and the species at *m*/*z* 1059.58 (+52.03 amu relative to 1007.55) are consistent with a lipid A molecule bearing two *N*-linked *R*-3-hydroxy-*cis*-vaccenate units, but this hypothesis remains to be verified with additional structural studies.

A similar series of higher mass peaks are seen both with the $[M - 2H]^{2-}$ ions (Figure 7B, black lines) of the lipid A species bearing two phosphate groups and with the $[M - H]^{-}$ ions of the 1-dephosphorylated lipid A species (Figure 7B, green lines). The M290A variant of LpxD is therefore responsible by itself for the

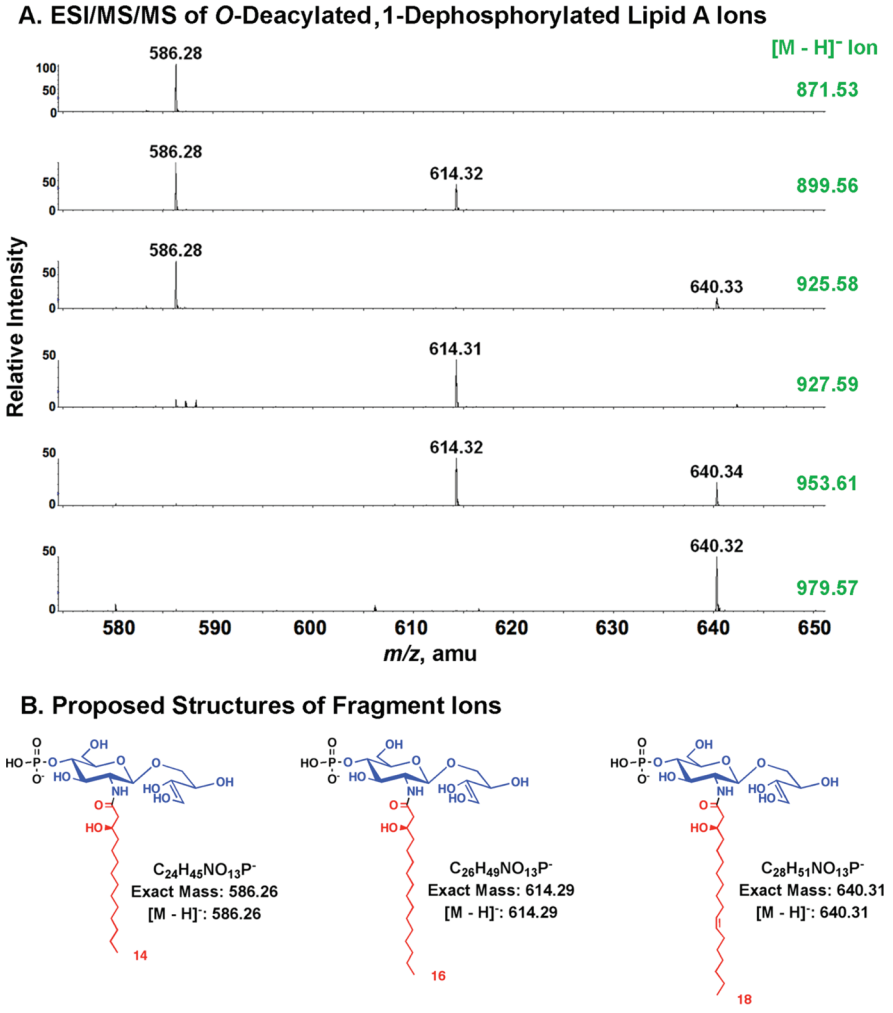

FIGURE 8: ESI/MS/MS analysis of *O*-deacylated and 1-dephosphorylated lipid A molecules obtained from RL25/pM290A. Panel A: Each of the singly charged monoisotopic ions indicated in green, which arise from the *O*-deacylated and 1-dephosphorylated lipid A molecules prepared from RL25/pM290A (Figure 7B, green lines), were subjected to MS/MS analysis. The relevant portions of the spectra containing the ions that arise by cross-ring cleavage of the proximal unit are shown. These fragmentation ions demonstrate that the M290A variant of EcLpxD is solely responsible for the incorporation of *N*-linked *R*-3-hydroxymyristoyl, *R*-3-hydroxypalmitoyl, and/or *R*-3-hydroxy-*cis*-vaccenoyl chains at both the 2 and 2′ positions of lipid A, consistent with Scheme 1. Panel B: Possible structures of the fragment ions giving rise to the peaks shown above. The actual material may consist of an isobaric mixture of related cross-ring cleavage products.

longer hydroxyacyl chains present in the lipid A of RL25/pM290A (Figure 6B).

Symmetrical Distribution of the N-Linked Hydroxyacyl Chains in RL25/pM290A Lipid A. The presence of some 1-dephosphorylated lipid A molecules (Figure 7) after combined mild-acid and mild-base treatment afforded an opportunity to evaluate the lengths of the hydroxyacyl chains attached to the 2′ position (Figure 8A). The 1-dephosphorylated lipid A species (Figure 7A, middle structure) undergo cross-ring cleavage of their proximal unit during collision-induced activation (*37*). The major fragment ions in the negative mode consists of the distal glucosamine unit with its amide-linked fatty acid at the 2′ position plus a portion of the proximal glucosamine ring (Figure 8B), permitting an unambiguous assessment of acyl chains present at the 2′ position.

MS/MS analysis of each of the $[M - H]^-$ ions (Figure 8A, green numbers) arising from the various 1-dephosphosphorylated species (Figure 7B, green lines) revealed the lengths of the *N*-linked hydroxyacyl chains attached to the distal glucosamine unit (Figures 8A and 8B). The fragmentation pattern is simple (Figure 8A) and provides additional evidence for the efficient incorporation of *N*-linked *R*-3-hydroxypalmitate and *R*-3-hydroxy-*cis*-vaccenate (in addition to some *R*-3-hydroxymyristate) by the M290A variant of EcLpxD (Figure 8B). The ion at *m*/*z* 871.53 (Figure 8A), which is the same as the major ion in wild-type lipid A (Figure 7A), gave rise to a single distal fragment at *m*/*z* 586.28 (Figure 8A), consistent with the presence of *R*-3-hydroxymyristate as the sole *N*-linked acyl chain at the 2′ position (Figure 8B). The ion at *m*/*z* 899.56 (Figure 8A) gave rise to two ions from the distal unit, one at *m*/*z* 586.28 presumed to contain *R*-3-hydroxymyristate, and the other at *m*/*z* 614.32, consistent with the incorporation of *R*-3-hydroxypalmitate. The fact that both of these ions arose from the same isobaric parent ion at *m*/*z* 899.56 demonstrates that the proximal unit must also contain a mixture of *N*-linked hydroxymyristate and hydroxypalmitate. The same considerations apply to the larger lipid A species of RL25/pM290A at *m*/*z* 925.58, 927.59, 953.61, and 979.57 (Figure 8A and 8B). These findings furthermore suggest that the *N*-acylation pattern of RL25/pM290A lipid A is fairly symmetrical, and that the downstream enzymes of the lipid A pathway do not select for or against the longer acyl chain variants produced by M290A EcLpxD.

Primary Sequence Patterns in Other LpxD Orthologues. Evidence that the region around the M290 side chain is involved

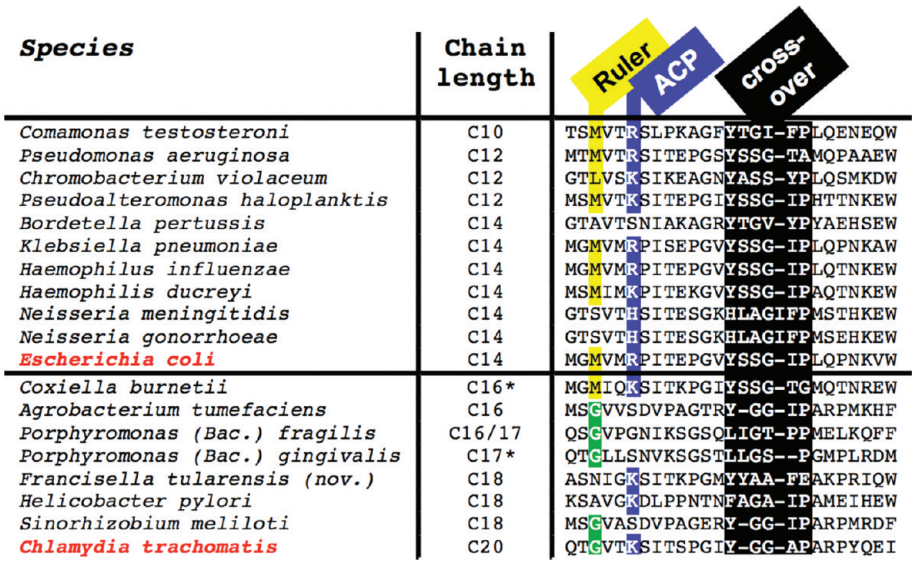

FIGURE 9: Conservation of the LpxD hydrocarbon ruler in Gram-negative bacteria. Primary sequence alignments of various LpxD orthologues were made using Kalign (*56*) and are grouped together with their predicted hydroxyacyl-ACP substrates, as inferred from the dominant acyl chains attached to the 2 and 2′ positions of their lipid As (*2*, *10*). The sequences are arranged from shortest acyl-chain length (top) to longest chain length (bottom). LpxDs that prefer fourteen-carbon or shorter hydroxyacyl-ACPs are above the line. LpxDs that prefer sixteen-carbon or longer hydroxyacyl-ACPs are below. The proposed hydrocarbon ruler region is highlighted with its methionine and leucine residues in yellow; the corresponding glycine residues of the longer chain selective LpxD variants are shown in green. Basic residues that have been proposed to interact with the hydroxyacyl-ACP donor substrate (*4*) are highlighted in blue. The region connecting the distal end of the LβH to the *C*-terminal domain (Figure 3) is highlighted in black. An asterisk denotes the possible presence of branched-chain fatty acids.

in determining the hydroxyacyl-ACP selectivity of LpxDs from other Gram-negative bacteria with known lipid A structures (*2*, *10*) was obtained by sequence comparisons. Figure 9 shows 19 LpxD sequences grouped by the dominant hydroxyacyl-chain attached to the 2 and 2′ positions of their lipid A. These sequences were divided into two groups, separated by the black line in Figure 9. The top 11 LpxDs are known (or presumed) to utilize 12- or 14-carbon hydroxyacyl-ACPs (*2*, *10*); the bottom 8 LpxDs are presumed to use 16-carbon (or longer) hydroxyacyl-ACPs. Consistent with the key role of the M290 side chain in determining the length of the hydroxyacyl chain incorporated by EcLpxD, 8 out of the 11 sequences in the top group contain a methionine or leucine side chain at the position equivalent to M290 of EcLpxD, and none have a glycine residue at this location. Furthermore, 5 of the 8 sequences in the lower group contain glycine at this position, as seen in CtLpxD. The only exception is LpxD from *Coxiella burnetii*. However, based on its lipid A structure, this LpxD orthologue is predicted to utilize a branched *R*-3-hydroxyacyl-ACP as its donor substrate (*38*).

DISCUSSION

Whereas most enzymes of lipid metabolism are integral membrane proteins (*39*−*41*), the first three enzymes of lipid A biosynthesis (LpxA, LpxC and LpxD) (Scheme 1) are soluble (*2*, *3*). Consequently, there has been considerable recent progress in determining their high-resolution structures (*5*) (*33*, *42*) (*43*−*45*). Buetow et al. reported the first crystal structure of an LpxD orthologue, that of *C. trachomatis* (Scheme 1B). Like *E. coli* LpxA (*33*), CtLpxD is a homotrimer (Figure 1) containing multiple hexad repeats. These units fold into a left-handed parallel β-helix (LβH), consisting of 18 amino acid residues per coil (*42*). Most proteins with LβH domains are homotrimers with three identical active sites located between adjacent pairs of subunits (Figure 1). Hexad repeats and their predicted LβH domains are easily identifiable in the primary sequences of proteins, many of which are hydroxyacyl, succinyl or acetyl transferases (*5*, *33*, *46*−*49*). *E. coli* K-12 contains at least eight proteins of this kind (*50*).

Based on the structure of *C. trachomatis* lipid A, CtLpxD is proposed to incorporate a *R*-3-hydroxyarachidoyl chain at the glucosamine 2 position of UDP-3-*O*-(myristoyl)-GlcN (Scheme 1B) (*12*). However, *in vitro* assays of CtLpxD have not been reported, and CtLpxD was not crystallized with a bound physiologically relevant substrate (*5*). It is therefore difficult to assess the roles of conserved residues in the mechanism of CtLpxD catalysis (*4*).

We have previously reported quantitative assays and extensive site-directed mutagenesis data for EcLpxD (*4*). We therefore determined the crystal structure of EcLpxD, which is highly selective for *R*-3-hydroxymyristoyl-ACP as its donor substrate (Scheme 1A) (*1*, *4*). The overall structure of EcLpxD is similar to that of CtLpxD (Figure 1), but the orientations of its *N*- and *C*-terminal domains relative to its LβH domain are different (Figures 1, 2 and 3). When the *N*-terminal domains are superpositioned by themselves, their structural similarity is more apparent (Figure 2D). Their different orientations relative to their associated LβH domains may be due to linker flexibility. The most striking difference between the conformations of the two proteins (Figures 2 and 3) is in the orientation of the crossover peptides between the LβH and *C*-terminal domains, resulting in a +120° rotation of the *C*-terminal domain relative to the LβH domain in EcLpxD versus CtLpxD (Figures 2 and 3). The function of the *C*-terminal domain is unknown, but its deletion results in complete loss of EcLpxD activity (*4*).

The locations of the proposed active sites and the positioning of the conserved catalytic residues EcLpxD H239 and CtLpxD247 are very similar (Figure 4A). The electron density in this region is strong for EcLpxD (Figure 4C). The H239A variant of EcLpxD has no residual catalytic activity (*4*), leading

to the proposed mechanism shown in Scheme 2, in which H239 functions as the catalytic base; this contrasts with the suggestion that H247 of CtLpxD might stabilize the oxyanion intermediate formed during the acylation process (*5*). Alternatively, we propose that the backbone *N*-atom of G257 (a residue conserved in all LpxDs) functions as part of the oxyanion hole (Scheme 2). As shown previously, even H125 and G143 of EcLpxA (the corresponding catalytic base and oxyanion hole) superposition nicely with H247 and G265 of CtLpxD (*4*). All LpxDs and LpxAs may share similar mechanisms of action.

In contrast to CtLpxD, there is no evidence for the presence of bound free fatty acids in EcLpxD (Figures 1, 2 and 4). The related hydrophobic cleft of EcLpxD, corresponding to the region where palmitate is bound in CtLpxD, is significantly smaller (Figure 4A). The M290 side chain of EcLpxD occludes the distal end of this cleft, which would interfere with the binding of fatty acids longer than fourteen carbon atoms (Figure 4A and 4C). The M290A variant of EcLpxD indeed prefers longer hydroxyacyl chains in its donor substrate, both *in vitro* (Table 2) and *in vivo* (Figures 6, 7 and 8). A methionine or a similarly bulky residue is conserved among most LpxD orthologues that prefer fourteen carbon or shorter hydroxyacyl-ACPs (Figure 9). This residue is replaced by glycine in CtLpxD and most other LpxD orthologues that utilize longer hydroxyacyl-ACPs (Figure 9).

We suggest that the palmitate-binding region on CtLpxD is the acyl chain-recognition site for *R*-3-hydroxyarachidoyl-ACP, and not of UDP-3-*O*-(myristoyl)-GlcN (*5*) (Scheme 1B). The location of the latter's acyl chain-binding site is uncertain. However, based on previous complementation studies, it is known that EcLpxD is not strictly *R*-3-hydroxymyristate dependent with regard to its acceptor substrate. Replacement of the *R*-3-hydroxymyristate-selective EcLpxA with the *R*-3-hydroxydecanoate-selective *Pseudomonas* LpxA results viable *E. coli* cells that the produce a hybrid lipid A molecule containing *R*-3-hydroxydecanoate at positions 3 and 3′, and *R*-3-hydroxymyristate at positions 2 and 2′ (*51*, *52*).

The observation that the longer-than-normal *N*-linked hydroxyacyl chains present in RL25/pM290A are equally distributed between the proximal and distal units of lipid A (Figure 8) shows that the downstream enzymes of the pathway, LpxH and LpxB (Scheme 1) (*3*), do not prefer one acyl chain length over another. The lengths of the acyl chains present in *E. coli* lipid A are determined primarily by acyltransferase selectivity, as seen in cells expressing the M290A variant of LpxD (Figures 6, 7 and 8); they are much less dependent upon the acyl-ACP pools. However, an interesting exception is seen in *E. coli* grown in the presence of propionate (*53*); these cells can prime their fatty acid biosynthetic pathway with either propionyl- or acetyl-coenzyme A, and thus generate significant quantities of odd-chain acyl-ACPs. A portion of the odd-numbered acyl chains is incorporated into lipid A under these conditions (*53*). EcLpxA and EcLpxD apparently cannot distinguish between acyl chains differing in length by only one carbon atom.

The LpxD acyltransferase may be a superior target for antibiotic design (*3*). Not only would cells fail to grow because they would not be able to make lipid A (*54*), but in addition the cells might accumulate the LpxC product UDP-3-*O*-(acyl)-GlcN, a potentially toxic, detergent-like molecule (Scheme 1) (*3*). ESI/MS studies indicate that this substance does indeed accumulate at 42 °C in RL25 (D. Zeng, C. M. Bartling and C. R. H. Raetz, unpublished). Potent inhibitors of LpxD have not been reported.

To understand the mechanism of EcLpxD in greater detail, it will be necessary to crystallize it together with a physiological ligand, such as *R*-3-hydroxymyristoyl-ACP or UDP-2,3-diacyl-GlcN (Scheme 1A). Most of the *E. coli* LpxA residues involved in substrate recognition are now known because structures with bound UDP-GlcNAc (*33*, *34*), UDP-3-*O*-(*R*-3-hydroxymyristoyl)-GlcNAc and (*R*-3-hydroxydecanoyl)-GlcNAc have been reported (*33*). Recent studies with *Leptospira interrogans* LpxA have provided further insights into sugar nucleotide selectivity and phosphopantetheine binding (*55*).

RL25/pM290A is the first example of an *E. coli* construct in which cells synthesize lipid A molecules with longer than normal *N*-linked hydroxyacyl chains. The composition of the outer membrane of RL25/pM290A, its permeability to small molecules, and the immunostimulatory properties of its lipid A may be altered in ways that might be useful for the development of novel vaccines.

ACKNOWLEDGMENT

We would like to thank Dr. James Phillips for help with X-ray diffraction experiments. We thank Drs. David Six, Ziqiang Guan and Sang Hoon Joo for their critical reading of the manuscript.

SUPPORTING INFORMATION AVAILABLE

A supplementary figure showing the amino acid sequence alignments of EcLpxD and CtLpxD; a table showing the differences in the lengths of the connecting loops between the secondary structural elements of the two proteins. This material is available free of charge via the Internet at http://pubs.acs.org.

REFERENCES

1. Kelly, T. M., Stachula, S. A., Raetz, C. R. H., and Anderson, M. S. (1993) The *firA* gene of *Escherichia coli* encodes UDP-3-*O*-(*R*-3-hydroxymyristoyl)-α-D-glucosamine *N*-acyltransferase: the third step of endotoxin biosynthesis. *J. Biol. Chem. 268*, 19866–19874.
2. Raetz, C. R. H., and Whitfield, C. (2002) Lipopolysaccharide endotoxins. *Annu. Rev. Biochem. 71*, 635–700.
3. Raetz, C. R. H., Reynolds, C. M., Trent, M. S., and Bishop, R. E. (2007) Lipid A modification systems in Gram-negative bacteria. *Annu. Rev. Biochem. 76*, 295–329.
4. Bartling, C. M., and Raetz, C. R. H. (2008) Steady-state kinetics and mechanism of LpxD, the *N*-acyltransferase of lipid A biosynthesis. *Biochemistry 47*, 5290–5302.
5. Buetow, L., Smith, T. K., Dawson, A., Fyffe, S., and Hunter, W. N. (2007) Structure and reactivity of LpxD, the *N*-acyltransferase of lipid A biosynthesis. *Proc. Natl. Acad. Sci. U.S.A. 104*, 4321–4326.
6. Takayama, K., Qureshi, N., Mascagni, P., Nashed, M. A., Anderson, L., and Raetz, C. R. H. (1983) Fatty acyl derivatives of glucosamine 1-phosphate in *Escherichia coli* and their relation to lipid A: complete structure of a diacyl GlcN-1-P found in a phosphatidylglycerol-deficient mutant. *J. Biol. Chem. 258*, 7379–7385.
7. Imoto, M., Yoshimura, H., Sakaguchi, N., Shimamoto, T., Kusumoto, S., and Shiba, T. (1987) Total synthesis of *Escherichia coli* lipid A, the endotoxically active principle of cell-surface lipopolysaccharide. *Bull. Chem. Soc. Jpn. 60*, 2205–2214.
8. Qureshi, N., Takayama, K., Mascagni, P., Honovich, J., Wong, R., and Cotter, R. J. (1988) Complete structural determination of lipopolysaccharide obtained from deep rough mutant of *Escherichia coli*. *J. Biol. Chem. 263*, 11971–11976.
9. Raetz, C. R. H. (1990) Biochemistry of endotoxins. *Annu. Rev. Biochem. 59*, 129–170.
10. Zähringer, U., Lindner, B., Rietschel, and E. T. (1999) Chemical structure of lipid A: recent advances in structural analysis of biologically active molecules, in Endotoxin in Health and Disease (Brade, H., Opal, S. M., Vogel, S. N., and Morrison, D. C., Eds.) pp 93−114, Marcel Dekker, Inc., New York.
11. Qureshi, N., Kaltashov, I., Walker, K., Doroshenko, V., Cotter, R. J., Takayama, K., Sievert, T. R., Rice, P. A., Lin, J. S., and Golenbock, D. T. (1997) Structure of the monophosphoryl lipid A moiety

obtained from the lipopolysaccharide of *Chlamydia trachomatis*. *J. Biol. Chem. 272*, 10594–10600.
12. Rund, S., Lindner, B., Brade, H., and Holst, O. (1999) Structural analysis of the lipopolysaccharide from *Chlamydia trachomatis* serotype L2. *J. Biol. Chem. 274*, 16819–16824.
13. Dicker, I. B., and Seetharam, S. (1991) Cloning and nucleotide sequence of the *firA* gene and the *firA200* allele from *E. coli*. *J. Bacteriol. 173*, 334–344.
14. Smith, P. K., Krohn, R. I., Hermanson, G. T., Mallia, A. K., Gartner, F. H., Provenzano, M. D., Fujimoto, E. K., Goeke, N. M., Olson, B. J., and Klenk, D. C. (1985) Measurement of protein using bicinchoninic acid. *Anal. Biochem. 150*, 76–85.
15. Kabsch, W. (1993) Automatic processing of rotation diffraction data from crystals of initially unknown symmetry and cell constants. *J. Appl. Crystallogr. 26*, 795–800.
16. McCoy, A. J., Grosse-Kunstleve, R. W., Storoni, L. C., and Read, R. J. (2005) Likelihood-enhanced fast translation functions. *Acta Crystallogr., Sect. D: Biol. Crystallogr. 61*, 458–464.
17. McCoy, A. J., Grosse-Kunstleve, R. W., Adams, P. D., Winn, M. D., Storoni, L. C., and Read, R. J. (2007) Phaser crystallographic software. *J. Appl. Crystallogr. 40*, 658–674.
18. Vagin, A., and Teplyakov, A. (1997) MOLREP: an automated program for molecular replacement. *J. Appl. Crystallogr. 30*, 1022–1025.
19. Emsley, P., and Cowtan, K. (2004) Coot: model-building tools for molecular graphics. *Acta Crystallogr., Sect. D: Biol. Crystallogr. 60*, 2126–2132.
20. Murshudov, G. N., Vagin, A. A., and Dodson, E. J. (1997) Refinement of macromolecular structures by the maximum-likelihood method. *Acta Crystallogr., Sect. D: Biol. Crystallogr. 53*, 240–255.
21. Adams, P. D., Grosse-Kunstleve, R. W., Hung, L. W., Ioerger, T. R., McCoy, A. J., Moriarty, N. W., Read, R. J., Sacchettini, J. C., Sauter, N. K., and Terwilliger, T. C. (2002) PHENIX: building new software for automated crystallographic structure determination. *Acta Crystallogr., Sect. D: Biol. Crystallogr. 58*, 1948–1954.
22. Davis, I. W., Murray, L. W., Richardson, J. S., and Richardson, D. C. (2004) MOLPROBITY: structure validation and all-atom contact analysis for nucleic acids and their complexes. *Nucleic Acids Res. 32*, W615–619.
23. Davis, I. W., Leaver-Fay, A., Chen, V. B., Block, J. N., Kapral, G. J., Wang, X., Murray, L. W., Arendall, W. B.3rd, Snoeyink, J., Richardson, J. S., and Richardson, D. C. (2007) MolProbity: all-atom contacts and structure validation for proteins and nucleic acids. *Nucleic Acids Res. 35*, W375–383.
24. Frishman, D., and Argos, P. (1995) Knowledge-based protein secondary structure assignment. *Proteins 23*, 566–579.
25. Guzman, L. M., Belin, D., Carson, M. J., and Beckwith, J. (1995) Tight regulation, modulation, and high-level expression by vectors containing the arabinose PBAD promoter. *J. Bacteriol. 177*, 4121–4130.
26. Miller, J. R. (1972) Experiments in Molecular Genetics , Cold Spring Harbor Laboratory, Cold Spring Harbor, NY.
27. Bligh, E. G., and Dyer, J. J. (1959) A rapid method of total lipid extraction and purification. *Can. J. Biochem. Physiol. 37*, 911–917.
28. Zhou, Z., White, K. A., Polissi, A., Georgopoulos, C., and Raetz, C. R. H. (1998) Function of *Escherichia coli* MsbA, an essential ABC family transporter, in lipid A and phospholipid biosynthesis. *J. Biol. Chem. 273*, 12466–12475.
29. Kanjilal-Kolar, S., and Raetz, C. R. H. (2006) Dodecaprenyl phosphate-galacturonic acid as a donor substrate for lipopolysaccharide core glycosylation in *Rhizobium leguminosarum*. *J. Biol. Chem. 281*, 12879–12887.
30. Raetz, C. R. H., Garrett, T. A., Reynolds, C. M., Shaw, W. A., Moore, J. D., Smith, D. C., Jr., Ribeiro, A. A., Murphy, R. C., Ulevitch, R. J., Fearns, C., Reichart, D., Glass, C. K., Benner, C., Subramaniam, S., Harkewicz, R., Bowers-Gentry, R. C., Buczynski, M. W., Cooper, J. A., Deems, R. A., and Dennis, E. A. (2006) Kdo$_2$-lipid A of *Escherichia coli*, a defined endotoxin that activates macrophages via TLR-4. *J. Lipid Res. 47*, 1097–1111.
31. Wang, X., Ribeiro, A. A., Guan, Z., Abraham, S. N., and Raetz, C. R. H. (2007) Attenuated virulence of a *Francisella* mutant lacking the lipid A 4′-phosphatase. *Proc. Natl. Acad. Sci. U.S.A. 104*, 4136–4141.
32. Wyckoff, T. J., and Raetz, C. R. H. (1999) The active site of *Escherichia coli* UDP-*N*-acetylglucosamine acyltransferase. Chemical modification and site-directed mutagenesis. *J. Biol. Chem. 274*, 27047–27055.
33. Williams, A. H., and Raetz, C. R. H. (2007) Structural basis for the acyl chain selectivity and mechanism of UDP-N-acetylglucosamine acyltransferase. *Proc. Natl. Acad. Sci. U.S.A. 104*, 13543–13550.
34. Ulaganathan, V., Buetow, L., and Hunter, W. N. (2007) Nucleotide Substrate Recognition by UDP-N-acetylglucosamine Acyltransferase (LpxA) in the First Step of Lipid A Biosynthesis. *J. Mol. Biol. 369*, 305–312.
35. Lathe, R., and Lecocq, J. P. (1977) The firA gene, a locus involved in the expression of rifampicin resistance in *Escherichia coli*. I. Characterisation of lambdafirA transducing phages constructed in vitro. *Mol. Gen. Genet. 154*, 43–51.
36. Touze, T., Tran, A. X., Hankins, J. V., Mengin-Lecreulx, D., and Trent, M. S. (2008) Periplasmic phosphorylation of lipid A is linked to the synthesis of undecaprenyl phosphate. *Mol. Microbiol. 67*, 264–277.
37. Six, D. A., Carty, S. M., Guan, Z., and Raetz, C. R. H. (2008) Purification and mutagenesis of LpxL, the Lauroyltransferase of *Escherichia coli* lipid A biosynthesis. *Biochemistry 47*, 8623–8637.
38. Toman, R., Garidel, P., Andra, J., Slaba, K., Hussein, A., Koch, M. H., and Brandenburg, K. (2004) Physicochemical characterization of the endotoxins from *Coxiella burnetii* strain Priscilla in relation to their bioactivities. *BMC Biochem. 5*, 1.
39. Raetz, C. R. H. (1986) Molecular genetics of membrane phospholipid synthesis. *Annu. Rev. Genet. 20*, 253–295.
40. Kent, C. (1995) Eucaryotic phospholipid synthesis. *Annu. Rev. Biochem. 64*, 315–343.
41. Cronan, J. E. (2003) Bacterial membrane lipids: where do we stand? *Annu. Rev. Microbiol. 57*, 203–224.
42. Raetz, C. R. H., and Roderick, S. L. (1995) A left-handed parallel ss helix in the structure of UDP-*N*-acetylglucosamine acyltransferase. *Science 270*, 997–1000.
43. Coggins, B. E., Li, X., McClerren, A. L., Hindsgaul, O., Raetz, C. R. H., and Zhou, P. (2003) Structure of the LpxC deacetylase with a bound substrate-analog inhibitor. *Nat. Struct. Biol. 10*, 645–651.
44. Whittington, D. A., Rusche, K. M., Shin, H., Fierke, C. A., and Christianson, D. W. (2003) Crystal structure of LpxC, a zinc-dependent deacetylase essential for endotoxin biosynthesis. *Proc. Natl. Acad. Sci. U.S.A. 100*, 8146–8150.
45. Mochalkin, I., Knafels, J. D., and Lightle, S. (2008) Crystal structure of LpxC from *Pseudomonas aeruginosa* complexed with the potent BB-78485 inhibitor. *Protein Sci. 17*, 450–457.
46. Beaman, T. W., Binder, D. A., Blanchard, J. S., and Roderick, S. L. (1997) Three-dimensional structure of tetrahydrodipicolinate *N*-succinyltransferase. *Biochemistry 36*, 489–494.
47. Olsen, L. R., and Roderick, S. L. (2001) Structure of the *Escherichia coli* GlmU pyrophosphorylase and acetyltransferase active sites. *Biochemistry 40*, 1913–1921.
48. Wang, X. G., Olsen, L. R., and Roderick, S. L. (2002) Structure of the *lac* operon galactoside acetyltransferase. *Structure* (*Cambridge*) *10*, 581–588.
49. Beaman, T. W., Sugantino, M., and Roderick, S. L. (1998) Structure of the hexapeptide xenobiotic acetyltransferase from *Pseudomonas aeruginosa*. *Biochemistry 37*, 6689–6696.
50. Blattner, F. R., Plunkett, G., Bloch, C. A., Perna, N. T., Burland, V., Riley, M., Collado-Vides, J., Glasner, J. D., Rode, C. K., Mayhew, G. F., Gregor, J., Davis, N. W., Kirkpatrick, H. A., Goeden, M. A., Rose, D. J., Mau, B., and Shao, Y. (1997) The complete genome sequence of *Escherichia coli* K-12. *Science 277*, 1453–1474.
51. Dotson, G. D., Kaltashov, I. A., Cotter, R. J., and Raetz, C. R. H. (1998) Expression cloning of a *Pseudomonas* gene encoding a hydroxydecanoyl-acyl carrier protein-dependent UDP-GlcNAc acyltransferase. *J. Bacteriol. 180*, 330–337.
52. Wyckoff, T. J. O., Lin, S., Cotter, R. J., Dotson, G. D., and Raetz, C. R. H. (1998) Hydrocarbon rulers in UDP-*N*-acetylglucosamine acyltransferases. *J. Biol. Chem. 273*, 32369–32372.
53. Bainbridge, B. W., Karimi-Naser, L., Reife, R., Blethen, F., Ernst, R. K., and Darveau, R. P. (2008) Acyl chain specificity of the acyltransferases LpxA and LpxD and substrate availability contribute to lipid A fatty acid heterogeneity in *Porphyromonas gingivalis*. *J. Bacteriol. 190*, 4549–4558.
54. McClerren, A. L., Endsley, S., Bowman, J. L., Andersen, N. H., Guan, Z., Rudolph, J., and Raetz, C. R. H. (2005) A slow, tight-binding inhibitor of the zinc-dependent deacetylase LpxC of lipid A biosynthesis with antibiotic activity comparable to ciprofloxacin. *Biochemistry 44*, 16574–16583.
55. Robins, L. I., Williams, A. H., and Raetz, C. R. H. (2009) Structural basis for the sugar nucleotide and acyl chain selectivity of *Leptospira interrogans* LpxA. *Biochemistry 48* (26), 6191–6201.
56. Lassmann, T., and Sonnhammer, E. L. (2006) Kalign, Kalignvu and Mumsa: web servers for multiple sequence alignment. *Nucleic Acids Res. 34*, W596–599.